Appl. Phys. A (2017) 123:518
DOI 10.1007/s00339-017-1101-4

Applied Physics A
Materials Science & Processing

Formation of slantwise orientated nanoscale ripple structures on a single-crystal 4H-SiC surface by time-delayed double femtosecond laser pulses

Wanlin He[1] · Jianjun Yang[1,2]

Received: 28 March 2017 / Accepted: 22 June 2017 / Published online: 14 July 2017

Abstract An effective control of the nanoscale periodic ripple structures on a single-crystal 4H-SiC surface is carried out by temporally delayed double collinear femtosecond laser pulse trains with different linear polarizations. The observed evolution of the ripple slant angle shows a dramatic decrease within an initial time delay range of ~10 ps between the two laser pulses, but keeps almost steady for larger time elapse. Through the detailed analyses, we propose a theoretical model to reveal the underlying physics: regarding the double femtosecond laser pulses, the first laser pulse transfers the semiconductor into nonequilibrium states associated with a transient refractive index grating on the surface, which subsequently tends to change the direction of the surface plasmon excitation of the second laser pulse. These behaviors can eventually result in the slantwise oriented laser intensity fringes and corresponding periodic ablation of grooves. Such investigations provide additional insights into the ripple formation processes, which is very important for control of nanomanufacturing materials by femtosecond lasers.

1 Introduction

Laser-induced periodic surface structures (LIPSS), also the so-called ripples, were first reported by Birnbaum on the surface of germanium in 1965 [1]. Ever since then, such a phenomenon has been evidenced on many kinds of materials such as metals, dielectric, and semiconductors because of the wide potential applications [2–8]. Numerous experiments showed that the LIPSS orientation strongly depends on the polarization of the incident laser beam, namely, it can be either perpendicular or parallel to the incident light polarization [9–12]. As for the formation mechanisms of the periodic ripple surface structures, an interference model between the incident laser and its excited surface plasmons has been developed and widely accepted by the researchers [13–15].

Under the single laser beam irradiation conditions, extensive efforts have been endeavored to manipulate the ripple structures through varying the incident femtosecond laser parameters (including the central wavelength, the energy fluence, number of pulses, and the polarization state) [16–19]. However, this kind of adjusting ability is very limited. Recently, many researchers have attempted to investigate the evolution of the surface structures with two time-delayed femtosecond laser pulse trains of either parallel or crossed linear polarizations. For example, they have found that both the orientation and the periodicity of the surface structures can be controlled by varying time delay of the inter-pulses [20]. Moreover, the available orientation of LIPSS was observed to slant with increasing the delayed incident laser fluence [21, 22]. Another common feature of the previous studies is that the time delay between two laser pulses was usually confined within a relatively small range (less than sub-ten picoseconds). Until now, the details of ripple formation by double time-delayed femtosecond laser pulse trains with other polarization intersection angles have not yet been explored.

In this work, by applying two collinearly propagated femtosecond laser pulses of different linear polarizations, we generate the nanoscale periodic ripple structures on a

✉ Jianjun Yang
jjyang@nankai.edu.cn

[1] Institute of Modern Optics, Nankai University, Tianjin 300071, China

[2] Changchun Institute of Optics, Fine Mechanics and Physics, Chinese Academy of Sciences, Changchun 130033, China

single-crystal 4H-SiC surface and modulate the spatial orientation through varying their time delays. The ripple slant is observed to undergo a rapid decrease within the first 10 ps followed by an abrupt transition into a steady regime. A physical model in terms of the surface wave excitation on a time-delay dependent transient index grating metasurface is proposed, which gives additional insights into the ripple formation mechanisms and indicates a new way to manipulate the surface structures with exploiting the nonequilibrium properties of the materials.

2 Experimental setup

Figure 1 presents a scheme of the experimental setup. A commercial chirped-pulse-amplification Ti: sapphire laser system (Spectra Physics, HP-Spitfire 50) was operated at 1 kHz to generate linearly polarized laser pulses of $\tau = 50$ fs time duration at a central wavelength of $\lambda = 800$ nm, and the maximum energy of a laser pulse was 2 mJ. In the experiment, each laser pulse out of the amplifier was separated into two pulses (P_1 and P_2) by a beam splitter (BS). A computer-controlled temporal delay Δt between the double pulses was varied in a range of 0–100 ps. During one of the beam paths, for example, the beam P_1, a half-wave plate was employed to change the direction of the laser linear polarization. After this, the double-pulse sequences were spatially collected into the collinear propagation and focused normally onto the surface of a single-side polished 4H-SiC (001) plate ($\sim$400 μm thickness) through a microscope objective lens (4×, N.A = 0.1). The sample was placed $\sim$300 μm away before reaching the focus, which leads to a Gaussian laser spot with a diameter (1/e intensity) of approximately 60 μm on the surface. The selection of the single-crystal SiC semiconductor is motivated by its unique physical properties and potential applications in high-temperature

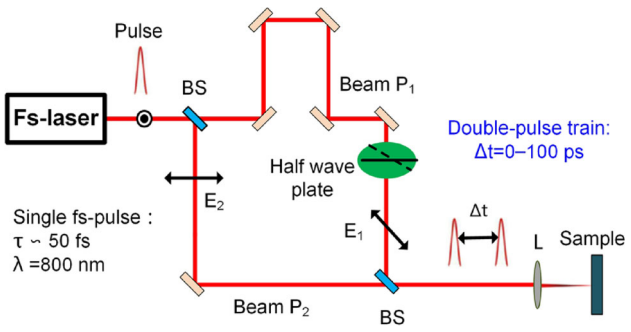

Fig. 1 Schematic diagram of the experimental setup. *BS* beam splitter; *fs* femtosecond; E_1 electric field of the laser beam P_1; E_2 electric field of the laser beam P_2; τ pulse width; λ center wavelength *L* microscope objective lens; Δt time delay between the double fs-laser pulses

electronic devices. All experiments were performed in ambient air by translating the sample at a speed of 0.1 mm/s, resulting in 600 laser pulses partially overlapped within one beam spot area. Before and after the experiments, the sample surface was ultrasonically cleaned in acetone solution. The surface morphology was observed with scanning electron microscopy (SEM).

3 Results and discussions

First, we investigated the surface morphologies of the sample irradiated by two isolated individual femtosecond laser beams at the same peak fluence of $F = 0.28$ J/cm^2, and the results are shown in Fig. 2a, b, respectively, where the intersection angle between the two laser linear polarizations is set as $\theta = 30°$. In the two cases, the periodic ripple structures were generated on the laser-irradiated surface, with the same periodicity of approximately $\Lambda = 150$ nm, which belong to the so-called high-spatial-frequency (HSF) LIPSSs [23]. Moreover, the spatial orientation of the ripple structures seems to be always perpendicular to the direction of the laser polarization in both cases, being consistent with the observations in previous studies [24–27]. When each laser pulse was attenuated to the lower peak fluence of $F = 0.12$ J/cm^2, no periodic ripple structures are generated on 4H-SiC crystal surface for the individual laser beam irradiation. However, if the double-pulse trains simultaneously arrived at the sample surface, i.e., the time delay between the two laser pulses $\Delta t = 0$ ps, it was surprisingly found that the periodic ripple structures can be formed on the sample surface, as shown in Fig. 2c. Under such circumstances the ripple orientation becomes neither perpendicular nor parallel to any directions of the two laser polarizations. The similar phenomenon has been also reported on the surface of titanium material [21]. If the ripple orientation (along the vertical direction) induced by the individual high-energy femtosecond laser beam P_2 in Fig. 2b is selected as reference direction, the available ripple structures are slantwise oriented with a degree of $\alpha = 19°$, slightly more than a half of the polarization intersection angle $\theta = 30°$. In other words, the growth of the ripple orientation is actually determined by both femtosecond laser pulses rather than by the individual ones. It should be pointed out that in our experiments, the width of the swath scribed by two spatially overlapped femtosecond laser beams was approximately 30 μm, and the ripple orientation across the entire damage region was found to slant in the same way, independent of the intensity variations within a Gaussian focal spot.

In addition, when double-pulse trains have crossed linear polarizations, there is no formation of the periodic ripple structures; instead we can only observe some

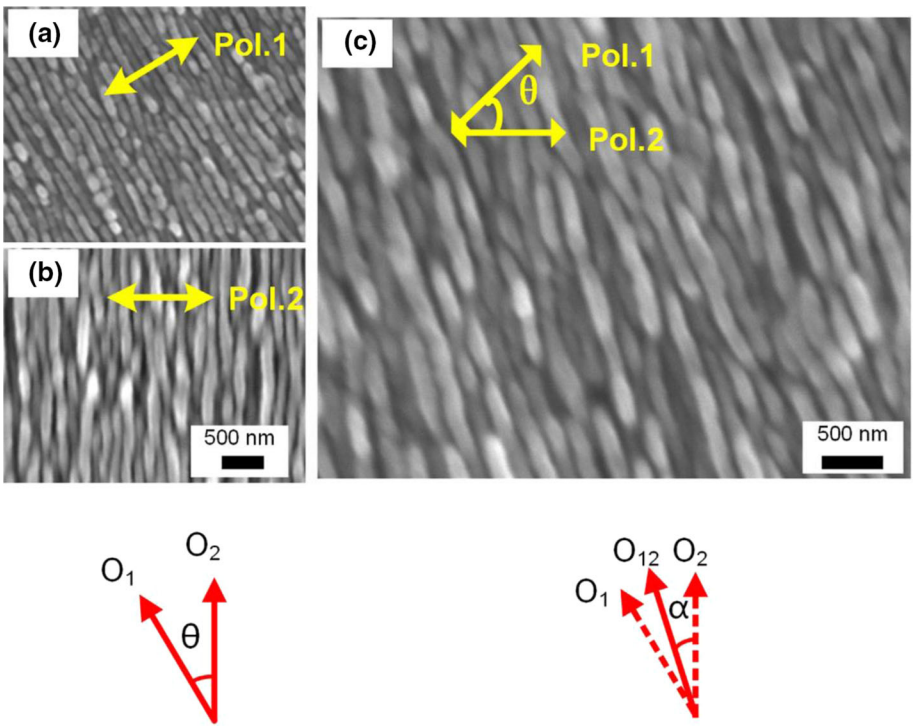

Fig. 2 **a**, **b** SEM images of the periodic ripple nanostructures formed on single-crystal 4H-SiC surface by two isolated individual femtosecond laser beams with different linear polarizations and the same peak fluence of $F = 0.28$ J/cm^2. **c** Ripple structures induced by the collinearly focused double-pulse trains at the time delay of $\Delta t = 0$ ps, where each laser peak fluence is $F = 0.12$ J/cm^2 and the intersection angle between directions of the two laser polarizations is $\theta = 30°$. *The yellow double arrows* (Pol.1 and Pol.2) denote polarizations of the two laser pulses, *the red single arrows* (O_1 and O_2) for the ripples orientations induced by the individual irradiation of two femtosecond laser beams, and the O_{12} represents the ripples orientation induced by two collinear femtosecond laser beams at zero time delay

nanoparticles on the laser-exposed surface region. It should be stressed here that when the linear polarizations of double-pulse trains are modulated parallel in the same direction, the induced ripple orientation was observed perpendicular to the laser polarization and can keep unchangeable even with either different either scanning speeds (within a range of 0.01–0.4 mm/s) or the inter-pulse time delays, which suggests that the varying overlaps of femtosecond laser pulse are not responsible for the orientation slant of the ripple structures.

Remarkably, the control of the ripples orientation was also demonstrated when the time delay of double-pulse trains was continuously varied within a range of 0–100 ps. In this case, the peak fluences of the two laser pulses are the same of $F = 0.12$ J/cm^2, and the laser pulse P_2, with linear polarization still along the horizontal direction, was temporally delayed. Figure 3 shows SEM images of the achieved ripple surface structures as a function of the time delay between the two laser beams and their fast Fourier transform images, when the polarization intersection angle is $\theta = 30°$. For the obtained fast Fourier transform images, the line shape of bright spots indicates an existence of the spatial period along this direction for the ripple structures, which is actually perpendicular to the ripple orientation. In the frequency domain, the ripple slant can be valued by the degree between the arrangement of the bright spots and the horizontal direction. Clearly, the ripples orientation becomes slantwise differently for variable time delays. For example, compared with the measured value of approximate $\alpha = 19°$ at $\Delta t = 0$ ps, the slant degree of the ripple orientation turns to be $\alpha = 16.9°$ at the larger time delay of $\Delta t = 2$ ps. If the time delay increases to $\Delta t = 10$ ps, the slant degree of the ripple orientation rapidly drops down to approximate $\alpha = 14.6°$. However, when the time delay between the two laser pulses spreads to $\Delta t = 20$ ps, the obtained slant degree of the ripple orientation reaches about $\alpha = 14°$, indicating a very slow decrease or the weaker physical influence of the first laser pulse P_1 on the ripple slant process. In particular, such kind of slow-varying tendency can continue to the larger time delay of 100 ps. Namely, the double-pulse induced ripple orientation keeps nearly invariant when the time delay becomes larger. Besides, given the above peak fluence, if the double-pulse trains are temporally delayed beyond 100 ps, no formation of the periodic ripple structures can be evidenced on the semiconductor surface.

Figure 4a shows a quantitative description of the ripple slant in terms of the time delay between the double-pulse

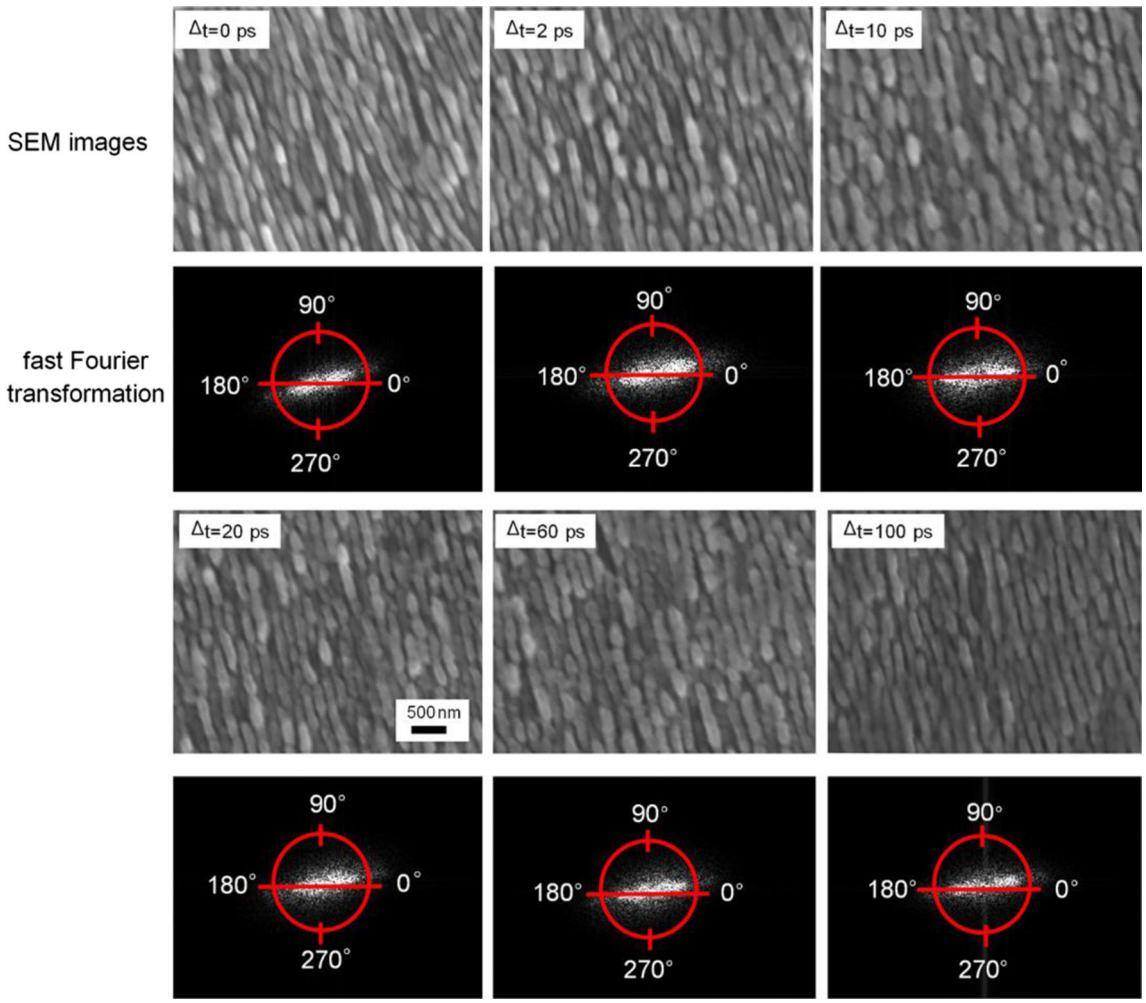

Fig. 3 SEM images and the corresponding fast Fourier transform images of the observed slant of the ripple structures on the single-crystal 4H-SiC surface upon irradiation of double-pulse trains with variable time delays. Here the polarization intersection angle is $\theta = 30°$, and the linear polarization of the second laser pulse P_2 is in the horizontal direction

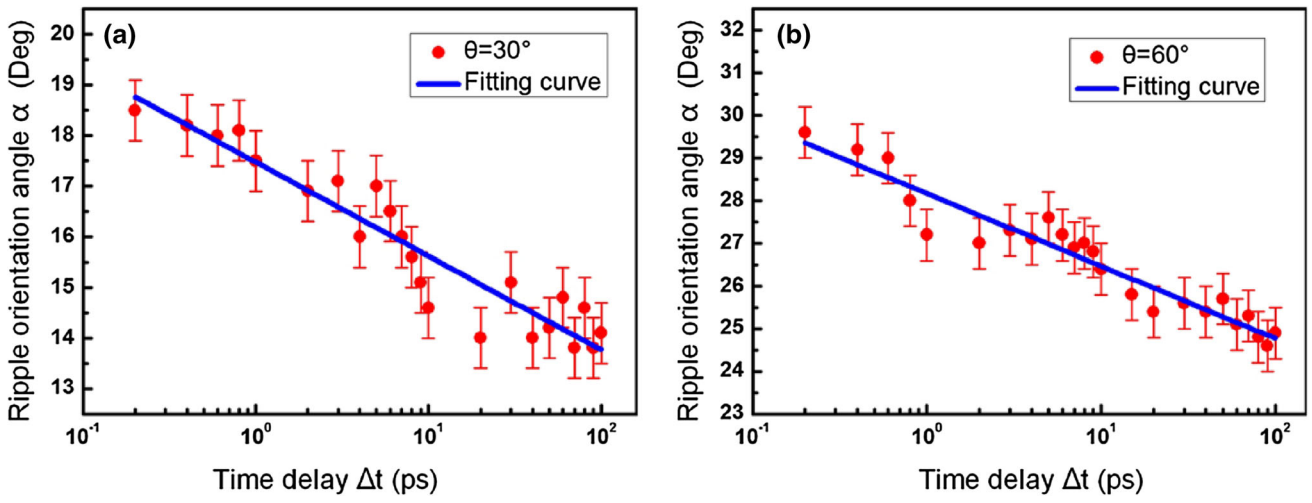

Fig. 4 Measured time delay dependence of the slant degree of the ripple orientation by double-pulse trains at different polarization intersection angles. **a** $\theta = 30°$; **b** $\theta = 60°$. *The solid blue lines* represent the fitting curves

trains. It can be seen that the variation of the slant degree presents a dramatic reduce during an initial time-delay range of $\Delta t = 0$–10 ps, but it turns to be almost steady for the larger time delays, which is much different from the observations on the metal targets [28]. Interestingly, when the polarization intersection angle was altered to other values such as $\theta = 60°$, a similar variation tendency can be still observed for the time delay dependent slant angle of the ripple orientation, as shown in Fig. 4b, although the magnitudes of the slant degree have different values. The larger the polarization intersection angle, the more pronounced the ripple slant becomes. The measured data of Fig. 4 were successfully fitted by a linear function of $a \sim (-t \times \Delta t_1) + A$ in logarithmical coordinates, where Δt_1 represents the decay time constant and A for an offset value. These parameters for difference cases are, respectively, given as follows: at $\theta = 30°$, $\Delta t_1 = 6.2$ ps and $A = 17.4°$; at $\theta = 60°$, $\Delta t_1 = 6.1$ ps and $A = 28.2°$.

4 Proposed physical model

The following scenario tries to elucidate the underlying physical mechanisms of the experimental observations. In the case of the single laser beam incidence, when the femtosecond laser pulses irradiate the sample, its optical interference with the excited surface plasmon leads to the spatially periodic distribution of the intensity patterns [13], which eventually generate permanent ripple grooves on sample surface via the material ablation processes. In the case of double-laser-beam incidence, when the collinear double-pulse trains irradiate the sample surface at the time delay of $\Delta t = 0$ ps, the two surface plasmons can be excited simultaneously on the same area of the sample surface, whose propagation directions are, respectively, parallel to the linear polarizations of the two laser pulses and the magnitudes of their wavevectors depend on the incident laser fluence. As a result, a new vector can be generated as a result of the sum of two surface plasmons, and its propagation direction is determined along the bisector of the polarization intersection angle, especially when the two laser pulses have the identical energy fluences, or the resultant slant degree of the periodic ripple structures equals $\theta/2$. Otherwise, the ripple slant deviates from $\theta/2$. This interpretation agrees well with the experimental observations in Fig. 2.

To have deep insights into the evolution of the measured slant degree of the ripple orientation with the time delay between double-pulse trains, we should consider the physical dynamic processes of the first femtosecond laser pulse P_1 irradiating the semiconductor surface. First of all, high-density free-electron plasma is generated in the laser-irradiated surface region via multiphoton absorption process upon femtosecond laser irradiation [29]. Subsequently, the surface plasmon can be excited and its interference with the incident laser leads to the intensity fringes and the periodic modulation of the optical properties on the sample surface. Therefore, a transient index grating can be formed with the grating vector $\boldsymbol{k}_g$ parallel to the direction of the linear polarization of the first laser pulse [30]. When the second laser pulse P_2 irradiates the sample, it is expected to couple with the transient metasurface of the periodic index grating. Because the two laser pulses are linearly polarized in different directions, there is an azimuth angle between the incident plane of the second laser pulse and the transient index grating, which is equal to the intersection angle between the two laser polarizations [31]. In other words, the wave vector of the second laser pulse projected on the sample surface has non-collinear alignment with the transient grating vector, as shown in Fig. 5. Therefore, the direction of surface plasmon excitation of the second laser pulse can be described by the following equation:

$$\tan \alpha = \frac{k_g \sin \theta}{k_{20} + k_g \cos \theta}, \tag{1}$$

where $\boldsymbol{k}_{20}$ is the wave vector projected on the sample surface of the second laser pulse P_2. Clearly, the direction of surface plasmon excitation (described by a slant degree of α with respective to the direction of the second laser polarization) closely depends on the transient grating vector $\boldsymbol{k}_g$.

In physical essence, the emergence of the transient index grating begins with the intensity fringes resulted from interference of the laser with its surface plasmon, and their subsequent optical heating processes cause some periodically excited regions with the high temperature of free-electron plasma within the beam spot, while other periodically spaced surface regions still remain in the equilibrium state. Under such circumstances, the dielectric constant variations are concentrated within the excited periodic regions. As discussed in the previous studies [32, 33], in semiconductors Auger recombination process plays an important role in reducing the number of laser-generated conduction band electrons at the surface, which consequently results in a dramatic change for the delay dependence of the dielectric constant of the material. Namely, with increasing time delay after the first pulse, the transient index grating k_g is rapidly decreased in the amplitude, as shown in Fig. 5c. According to Eq. (1), the obtained ripple slant angle α also becomes decreased. However, as the relaxation time goes beyond $\sim$10 ps, the change of the temperature-induced dielectric constant becomes much slow because of the weak thermal conductivity for the semiconductor material, thus making a long-term sustainability of the transient index grating patterns, which is

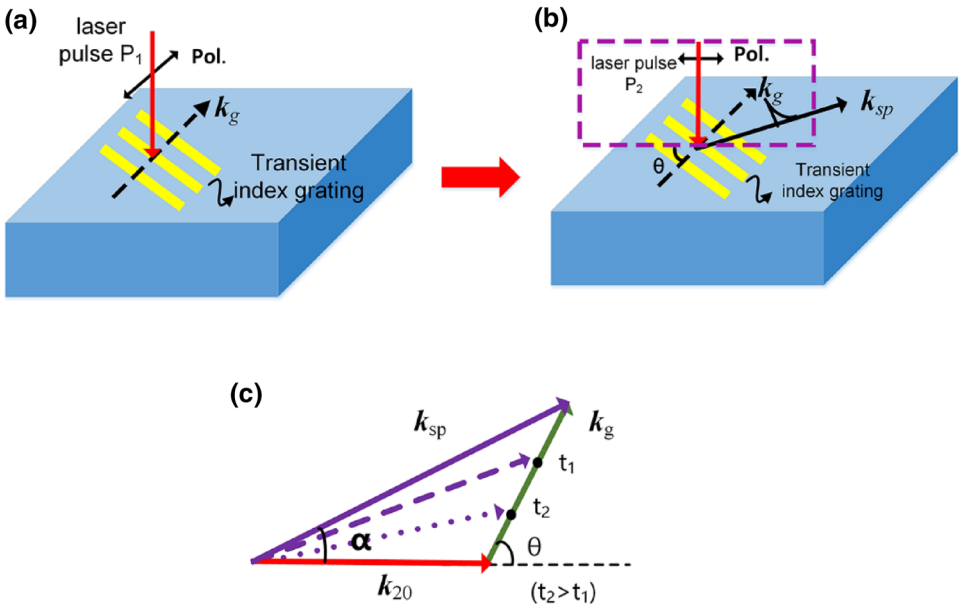

Fig. 5 Proposed physical model for the ripple slant upon irradiation of two time-delayed femtosecond laser pulses with different linear polarizations. **a** Diagram of ultrafast physical processes happening on the semiconductor surface, on which a spatially periodic transient index grating is firstly created by the first laser pulse. **b** The surface plasmon excitation of the second laser pulse is affected by the transient index grating patterns on the surface to deviate from the direction of its incident laser polarization, thereby making ripple orientation become slantwise. **c** A vector diagram for the direction of the surface plasmon excitation ($\boldsymbol{k}_{sp}$) when the second laser pulse ($\boldsymbol{k}_{20}$) is coupled with the transient grating vector ($\boldsymbol{k}_{g}$) at different time delays ($t_2 > t_1$)

consistent with the experimentally observed steady regime in the slant degree of the ripple orientation (It should be here noted that in the experiments, we have also investigated the slant situations of the ripple structures formed on the copper metal, and found that the ripple slant degree would only exist within the time delay range less than 40 ps, without displaying any nonzero values of the steady regime [28]). More specifically, regarding to the time dependent slant degree of the ripple orientation, the observed dramatic reduce process indicates a strong change of the dielectric constant in the sample surface; while the steady regime suggests the sustainability of the transient index grating metasurface.

5 Conclusions

In summary, we have generated the ripple structures by irradiating the semiconductor 4H-SiC crystal surface with the time-delayed double-pulse trains, which collinearly propagate at different linear polarizations. Orientation of the ripple structures has been found to monotonically slant when the time delay of the inter-pulse is varied. Remarkably, the observed ripple slant angle exhibits a steady variation regime after undergoing a short-term ($\sim$10 ps) rapid decreasing tendency, even for several intersection angles between the two laser polarizations. The physics of the ripple slant is attributed to the coupling of the femtosecond laser pulse with the transient metasurface of the optically excited semiconductor, specifically, the irradiation of the first femtosecond laser pulse produces grating-like changes of the optical index on the sample surface via the surface plasmon excitation. The temporal relaxation of such a transient index grating subsequently affects the direction of surface plasmon excitation of the second femtosecond laser pulse, finally resulting in the periodically ablated grooves with the slantwise orientation. Our investigations have proposed an effective method to control the formation of the ripple structures, which benefits the design and fabrication of nanoscale devices on material surfaces.

Acknowledgements The authors acknowledge the financial support for this work provided by the Natural National Science Foundation of China (NSFC) (11274184, 11674178), Tianjin National Natural Science Foundation (12JCZDJC20200) and Research Fund for the Doctoral Program of higher Education of China (20120031110032).

References

1. M. Birnbaum, J. Appl. Phys. **36**, 3688 (1965)
2. Y. Tang, J. Yang, B. Zhao, M. Wang, X. Zhu, Opt. Express **20**, 25826 (2012)
3. L. Qi, K. Nishii, Y. Namba, Opt. Lett. **34**, 1846 (2009)
4. R. Wagner, J. Gottmann, A. Horn, E.W. Kreutz, Appl. Surf. Sci. **252**, 8576 (2006)
5. R. Kuladeep, C. Sahoo, D.N. Rao, Appl. Phys. Lett. **104**, 222103 (2014)

6. A.Y. Vorobyev, C. Guo, Appl. Phys. Lett. **92**, 041914 (2008)
7. T. Baldacchini, J.E. Carey, M. Zhou, E. Mazur, Langmuir **22**, 4917 (2006)
8. A. Mizuno, T. Honda, J. Kiuchi, Y. Iwai, N. Yasumaru, K. Miyazaki, Tribol. Online **1**, 44 (2006)
9. L. Xue, J. Yang, Y. Yang, Y. Wang, X. Zhu, Appl. Phys. A **109**, 357 (2012)
10. J. Bonse, M. Munz, H. Sturm, J. Appl. Phys. **97**, 013538 (2005)
11. A.Y. Vorobyev, C. Guo, J. Appl. Phys. **104**, 063523 (2008)
12. J.F. Young, J.S. Preston, H.M. van Driel, J.E. Sipe, Phys. Rev. B **27**, 1155 (1983)
13. M. Huang, F. Zhao, Y. Cheng, N. Xu, Z. Xu, ACS Nano **3**, 4062 (2009)
14. J. Bonse, A. Rosenfeld, J. Krüger, J. Appl. Phys. **106**, 104910 (2009)
15. F. Garrelie, J.P. Colombier, F. Pigeon, S. Tonchev, N. Faure, M. Bounhalli, S. Reynaud, O. Parriaux, Opt. Express **19**, 9035 (2011)
16. M. Huang, F. Zhao, Y. Cheng, N. Xu, Z. Xu, Phys. Rev. B **79**, 125436 (2009)
17. J. Bonse, J. Krüger, J. Appl. Phys. **108**, 034903 (2010)
18. Y. Yang, J. Yang, L. Xue, Y. Guo, Appl. Phys. Lett. **97**, 141101 (2010)
19. X. Li, W. Rong, L. Jiang, K. Zhang, C. Li, Q. Cao, G. Zhang, Y. Lu, Opt. Express **22**, 30170 (2014)
20. M. Rohloff, S.K. Das, S. Höhm, R. Grunwald, A. Rosenfeld, J. Krüger, J. Bonse, J. Appl. Phys. **110**, 014910 (2011)
21. M. Hashida, T. Nishii, Y. Miyasaka, H. Sakagami, M. Shimizu, S. Inoue, S. Sakabe, Appl. Phys. A **122**, 484 (2016)
22. T. Jia, H. Chen, M. Huang, F. Zhao, J. Qiu, R. Li, Z. Xu, X. He, J. Zhang, H. Kuroda, Phys. Rev. B **72**, 10 (2005)
23. J. Yao, C. Zhang, H. Liu, Q. Dai, L. Wu, S. Lan, A.V. Gopal, V.A. Trofimov, T.M. Lysak, Opt. Express **20**, 905 (2012)
24. Y. Ma, V. Khuat, A. Pan, Opt. Laser. Eng. **82**, 141 (2016)
25. T. Tomita, K. Kinoshita, S. Matsuo, S. Hashimoto, Appl. Phys. Lett. **90**, 153115 (2007)
26. M. Yamaguchi, S. Ueno, R. Kumai, K. Kinoshita, T. Murai, T. Tomita, S. Matsuo, S. Hashimoto, Appl. Phys. A **99**, 23 (2010)
27. J. Song, W. Tao, H. Song, M. Gong, G. Ma, Y. Dai, Q. Zhao, J. Qiu, Appl. Phys. A **122**, 341 (2016)
28. B. Zhao, J. Yang, X. Zhu, X. Xu, F. Xie, Surface dynamics of warm dense copper metal captured in femtosecond laser-induced deflecting ripple structures. N. J. Phys. (2017) (**in revision**)
29. G. Obara, H. Shimizu, T. Enami, E. Mazur, M. Terakawa, M. Obara, Opt. Express **21**, 26323 (2013)
30. J. Cong, J. Yang, B. Zhao, X. Xu, Opt. Express **23**, 5357 (2015)
31. S.J. Elston, G.P. Bryan-Brown, J.R. Sambles, Phys. Rev. B **44**, 6393 (1991)
32. S. Höhm, A. Rosenfeld, J. Krüger, J. Bonse, Appl. Surf. Sci. **278**, 7 (2013)
33. T.J.-Y. Derrien, J. Krüger, T.E. Itina, S. Höhm, A. Rosenfeld, J. Bonse, Appl. Phys. A **117**, 77 (2014)